International Journal of Engineering Research and Development
e- ISSN: 2278-067X, p-ISSN: 2278-800X, www.ijerd.com
Volume 22, Issue 5 (May 2026), PP 483-498

Simulation of Waste to Energy Plant Using Flue Gas from Fluid Catalytic Cracking Regenerator

[1] Atukpa ThankGod Ayibabrakaemi [2] Dagde, K.K[3] Ehirim, E.O.
[1, 2, 3,] Department of Chemical/Petrochemical Engineering, Faculty of Engineering, Rivers State University, Nigeria

Abstract
This study presents the simulation, performance analysis, and validation of a waste-to-energy plant integrated with a fluid catalytic cracking (FCC) regenerator using Aspen HYSYS. The system comprises a gas expander, a heat recovery steam generator (economizer, evaporator, and superheater), a steam turbine–generator, and a condenser for effective recovery of thermal energy from FCC flue gas. Detailed material and energy balances confirmed thermodynamic consistency across all units. The FCC regenerator flue gas entered the system at a temperature of 700 °C and pressure of 250 kPa with a mass flow rate of 3 × 10^5 kg/h, providing a heat flow of approximately −5.45 × 10^8 kJ/h.The gas expander reduced the flue gas temperature from 700 °C to 585.3 °C and pressure from 250 kPa to 120 kPa, generating about 27.19 MW of mechanical power with a polytropic efficiency of 85%. Subsequent heat recovery through the economizer lowered flue gas temperature to 519.2 °C while heating boiler feedwater from 105 °C to 230 °C. The evaporator further cooled the gas to 507.1 °C and produced saturated steam at 250 °C and 4000 kPa, which was then superheated to 442.4 °C in the superheater as the flue gas exited to the stack at 251 °C. The steam turbine expanded the superheated steam from 4000 kPa and 442.4 °C to 10 kPa and 46.01 °C, producing approximately 26.52 MW of power with a polytropic efficiency of 86%. Condensation of exhaust steam was achieved at 25.01 °C using cooling water heated from 20 °C to 35 °C. Sensitivity analysis showed that expander efficiency increased slightly from about 73.11% to 73.56% as flue gas temperature rose from 110 °C to 1910 °C, while expander power output increased significantly from about 5.96 MW to 34.79 MW. At constant temperature, expander efficiency remained constant at approximately 73.33% as mass flow rate increased from 1 × 10^5 kg/h to 1 × 10^6 kg/h, while power output increased linearly from 3.83 MW to 38.34 MW. For the steam turbine–generator, efficiency increased from about 60.12% to 71.96% as flue gas temperature rose from 810 °C to 1910 °C, and power output increased from 21.74 MW to 70.60 MW. Increasing flue gas mass flow rate from 5 × 10^5 kg/h to 1 × 10^6 kg/h raised generator efficiency from 59.89% to 63.71% and power output from 20.35 MW to 46.03 MW. Economic analysis yielded a total capital cost of USD 2.82 million, total operating cost of USD 1.51 million per year, and total utility cost of USD 180,182 per year, indicating economic viability. Model validation against plant data showed good agreement, with deviations generally below 5% for key parameters such as efficiency, power output, outlet temperature, and pressure. Overall, the study demonstrates that FCC regenerator flue gas can be effectively harnessed to generate substantial electrical power, improve refinery energy efficiency, and reduce waste heat losses, providing a technically and economically viable pathway for sustainable refinery operation.

Keywords*: Waste heat recovery; FCC regenerator; Flue gas; Aspen HYSYS; Power generation*

Date of Submission: 13-05-2026 Date of acceptance: 28-05-2026

I. INTRODUCTION

The global energy landscape is shifting rapidly in response to climate change, depleting fossil fuels, and the need for sustainable industrial operations. In refining industries, Fluid Catalytic Cracking (FCC) units are vital for converting heavy oil fractions into more valuable light products. However, these units generate high-temperature flue gases during the regeneration of catalysts, which are typically released into the atmosphere, contributing to environmental pollution and energy waste (Luan *et al*., 2020).

Nigeria, one of the leading oil-producing nations in Africa, possesses a substantial refining capacity, with several state-owned and private refineries distributed across the country. These facilities play a pivotal role in meeting domestic energy demand and supporting economic development. A critical component of modern refineries is the Fluid Catalytic Cracking (FCC) unit, which serves to convert heavy fractions of crude oil into more valuable lighter hydrocarbons such as gasoline and olefins. During the regeneration stage of the FCC process, coke deposited on the catalyst is burned off, producing high-temperature flue gas as a byproduct (Honeywell, 2023).

The flue gas from FCC regenerators typically contains a mixture of nitrogen, carbon dioxide (CO_2), oxygen, water vapor, and trace amounts of pollutants such as sulfur oxides (SOx), nitrogen oxides (NOx), ammonia (NH_3), hydrogen cyanide (HCN), and volatile organic compounds (VOCs). According to Honeywell (2023), CO_2 concentrations in FCC flue gas can range between 15–20%, while the remaining composition consists mainly of nitrogen and steam. This gas, often vented to the atmosphere through stacks or exhaust systems, carries significant thermal energy that remains largely unutilized in many refineries.

In Nigeria, the problem of energy inefficiency is widespread across the industrial sector, including the refining industry. Many refineries still operate with outdated infrastructure and lack modern systems for energy recovery. As highlighted by Onwu (2020), a substantial portion of energy used in industrial processes is lost as waste heat. This includes thermal energy from flue gases, hot effluent streams, and exhausts. In the context of FCC units, recovering heat from flue gas offers an untapped opportunity to enhance energy efficiency, reduce fuel consumption, and contribute to environmental sustainability.

Waste-to-energy (WTE) systems offer a promising approach for recovering this energy. Bottoming cycles such as the steam Rankine cycle or the Organic Rankine Cycle (ORC) are particularly well-suited for harnessing the thermal potential of medium-temperature flue gases. These systems can convert waste heat directly into electricity by expanding a working fluid through a turbine, thus producing usable power without additional fuel consumption. The advantage of ORCs lies in their ability to operate at lower temperatures using organic fluids, making them ideal for integration with FCC flue gas recovery systems (Sadek *et al*., 2023).

Advancements in process simulation tools have enabled the modeling of complex energy recovery systems before physical implementation. Aspen HYSYS, one of the leading process modeling environments, allows for detailed design and thermodynamic analysis of chemical and power systems. By simulating a waste-to-energy recovery unit using FCC flue gas as the heat source, it is possible to predict system performance, optimize process parameters, and evaluate technical feasibility. Furthermore, simulation supports economic analysis by providing data for capital and operational cost estimation, power output, and efficiency metrics (Gulec *et al*., 2018).

Given the urgent need to enhance energy utilization and environmental sustainability in Nigeria's refining sector, this study aims to develop a simulation model for electricity generation using FCC flue gas. The project focuses on the application of Aspen HYSYS to simulate an HRSG-based plant capable of harnessing waste heat for power production. By leveraging simulation outcomes and economic indicators, the study provides a framework for integrating energy recovery technologies in Nigerian refineries, contributing to national energy security and emissions reduction goals.

II. EXTENT OF PAST WORKS

(Zhang *et al*., 2020), carried out a study to investigate energy efficiency improvement in fluid catalytic cracking (FCC) units through waste heat recovery from regenerator flue gas. A detailed thermodynamic model was developed to quantify recoverable heat and potential power generation. The results showed that significant energy savings could be achieved by integrating waste heat recovery systems into FCC operations, thereby reducing overall refinery energy consumption. The authors concluded that FCC regenerator flue gas represents a high-grade energy source and that proper heat recovery integration can substantially improve refinery energy efficiency and sustainability.

(Liu *et al*., 2018), in this work analyzed a combined gas–steam turbine system for industrial waste heat recovery using thermodynamic simulation. The study demonstrated that coupling gas expansion with steam power cycles enhances total power output and system efficiency compared to single-cycle configurations It was concluded that combined-cycle configurations provide superior energy recovery performance and are well suited for high-temperature industrial flue gas applications.

(Campana *et al*., 2013), in this work the authors evaluated waste heat recovery technologies across European energy-intensive industries, focusing on organic Rankine cycles and steam-based systems. Performance indicators such as power output, efficiency, and economic feasibility were assessed. The study concluded that waste heat recovery systems are technically feasible and economically attractive for large-scale industrial plants with continuous high-temperature exhaust streams.His research assessed the performance of heat recovery steam generators under varying operating conditions. The study examined how fluctuations in flue gas temperature and flow rate affect steam production and thermal efficiency. The authors concluded that HRSG performance is strongly dependent on inlet flue gas conditions, emphasizing the need for flexible design to handle operational variability (Hou *et al*., 2021).

(Sánchez *et al*., 2019) carried out a thermodynamic assessment of different HRSG configurations for industrial waste heat recovery was conducted. Multiple layouts were compared based on energy efficiency and heat utilization effectiveness. The study concluded that multi-pressure HRSG configurations outperform single-pressure systems in maximizing heat recovery from industrial exhaust gases.

(Di Bona & Forcina, 2017), This study focused on availability and efficiency analysis of industrial steam power plants using exergy-based methods. Losses in turbines, condensers, and heat exchangers were quantified. The authors concluded that steam turbines and condensers are major sources of irreversibility, and improving their design can significantly enhance overall plant efficiency. The authors developed and optimized waste heat recovery systems using Aspen HYSYS.

(Pan *et al*., 2021), The study evaluated the influence of operating conditions on system efficiency and power output. It was concluded that process simulation tools such as Aspen HYSYS are reliable for optimizing waste heat recovery systems and predicting plant performance.

(Wang *et al*., 2022), this research modeled steam turbine power cycles for industrial waste heat recovery, focusing on performance indicators such as efficiency, power output, and expansion. The study concluded that steam turbine performance improves significantly with higher steam inlet temperature and pressure, consistent with Rankine cycle theory.

(Jouhara *et al*., 2018), this review examined heat pipe-based systems for waste heat recovery across industrial applications. The advantages of compactness, efficiency, and operational flexibility were highlighted. The authors concluded that heat pipes are effective components for low- and medium-temperature waste heat recovery systems.

This paper reviewed energy efficiency and energy-saving opportunities in compressed air and industrial energy systems, including waste heat recovery technologies (Saidur *et al*., 2010).The study concluded that industrial energy efficiency can be significantly improved through systematic waste heat recovery and optimization strategies .

(Li *et al*., 2019), The authors performed thermodynamic analysis of waste heat recovery systems using energy and exergy methods to evaluate performance limits. It was concluded that exergy analysis provides deeper insight into inefficiencies and is essential for optimal system design (Li *et al*., 2019).

(Karellas *et al*., 2013), this study analyzed the energetic and energetic performance of waste heat recovery systems applied to industrial plants The authors concluded that combining energy and exergy analysis leads to more realistic evaluation of waste heat recovery potential.

(Gungor & Erbay, 2019), The performance of steam turbines under varying operating conditions was analyzed using experimental and modeling approaches .The study concluded that turbine efficiency and power output are highly sensitive to inlet steam conditions and load variations.

(Liu *et al*., 2020), this research evaluated energy and exergy performance of refinery waste heat recovery systems with emphasis on sustainability The authors concluded that refinery waste heat recovery significantly reduces energy losses and environmental impact.

(Ahmadi *et al*., 2011), a combined gas–steam power cycle was thermodynamically modeled and optimized using energy and exergy analysis The study concluded that optimized combined cycles outperform conventional systems in efficiency and power generation. The authors concluded that high-temperature waste heat offers the greatest potential for power generation using steam and gas turbines.

(Wang *et al*., 2011), in this study analyzed combined gas–steam cycle performance under different operating scenarios It was concluded that combined-cycle configurations significantly improve thermal efficiency compared to single-cycle systems.

(Bejan & Tsatsaronis, 1996), this paper introduced thermodynamic optimization concepts for energy systems using exergy analysis The authors concluded that minimizing irreversibilities is key to improving energy system performance (Bejan & Tsatsaronis, 1996).This study explored power generation from industrial flue gas waste heat using steam-based cycles (Xu *et al*., 2017).The authors concluded that industrial flue gas can be effectively converted into electricity using properly designed recovery systems.

(Yu *et al*., 2020) an exergy-based evaluation of refinery waste heat recovery systems was conducted to identify efficiency improvement opportunities The study concluded that exergy analysis is a powerful tool for enhancing the design and optimization of refinery waste heat recovery systems (Yu *et al*., 2020).

III. MATERIALS AND METHOD

2.1 Materials Used

The materials used in this research work were data from DANGOTE Refinery and include the following:

i. Inlet feed operating conditions and Comprehensive feed compositions
ii. Chemical Engineering Software (Aspen Hysys version 14)

2.2 Method used

The methods that were applied in this study includes:

2.2.1 Material and Energy Balance Design Equations of Major Equipment

2.2.1.1 Compressor Design Equations

Steady-Flow Energy Equation (First Law)

$\dot{Q} - \dot{W}_s = \dot{m}[(h_2 - h_1) + (V_2^2 - V_1^2)/2 + g(z_2 - z_1)]$ (1)

Where:

$\dot{Q}$ = rate of heat transfer to the compressor (W)

$\dot{W}_s$ = shaft work rate (W)

$\dot{m}$ = mass flow rate (kg/s)

h_1, h_2 = specific enthalpy at inlet and outlet (J/kg)

V_1, V_2 = fluid velocity at inlet and outlet (m/s)

z_1, z_2 = elevation at inlet and outlet (m)

g = acceleration due to gravity (m/s²)

Neglecting kinetic and potential energy changes

$\dot{Q} - \dot{W}_s = \dot{m}(h_2 - h_1)$ (2)

Where:

All symbols are as previously defined.

This assumption is valid for most industrial compressors.

Adiabatic compressor ($\dot{Q} \approx 0$)

$-\dot{W}_s = \dot{m}\ (h_2 - h_1)$ (3)

Where:

The compressor is assumed thermally insulated.

Specific compressor work

$w = h_2 - h_1$ (4)

Where:

w = specific compressor work (J/kg)

Enthalpy–temperature relation (ideal gas)

$dh = C_p\ dT$ (5)

Where:

C_p = specific heat capacity at constant pressure (J/kg·K)

T = absolute temperature (K)

Integrated enthalpy change

$h_2 - h_1 = \int_{T_1}^{T_2} C_P\ dT$ (6)

Where:

T_1, T_2 = inlet and outlet temperatures (K)

Constant heat-capacity assumption

$h_2 - h_1 = C_p(T_2 - T_1)$ (7)

Where:

C_p is assumed constant over the temperature range.

Entropy relation for an ideal gas

$ds = C_p(\frac{dT}{T}) - R(\frac{dP}{P})$ (8)

Where:

s = specific entropy (J/kg·K)

R = universal gas constant (J/kg·K)

P = pressure (Pa)

Isentropic compression (reversible adiabatic)

$ds = 0$

Where:

Entropy remains constant during ideal compression.

Integrated isentropic temperature–pressure relation

$\ln(\frac{T_2}{T_1}T_2/T_1) = (R/C_p)\ \ln(\frac{P_2}{P_1})$ (9)

Where:

P_1, P_2 = inlet and outlet pressures (Pa)

Isentropic temperature relation

$\frac{T_{2s}}{T_1} = \left(\frac{P_2}{P_1}\right)^{\left(\frac{k-1}{k}\right)}$ (10)

Where:

T_2s = outlet temperature for isentropic compression (K)

k = ratio of specific heats (C_p/C_v)

Compressor isentropic efficiency

$\eta_c = \frac{(h_2 s - h_1)}{(h_2 - h_1)}$ (11)

Where:
ηc = compressor isentropic efficiency
h_2s = outlet enthalpy for isentropic compression (J/kg)
Actual temperature rise

$$T_2 - T_1 = \frac{(T_2s - T_1)}{\eta_c} \quad (12)$$

Where:
T_2 = actual outlet temperature (K)

2.2.1.2 Expander / Turbine Design Equations

Energy balance (adiabatic turbine)

$$\dot{W}_s = \dot{m}(h_1 - h_2) \quad (13)$$

Where:
$\dot{W}_s$ = power produced by turbine (W)
Specific turbine work

$$w = h_1 - h_2 \quad (14)$$

Where:
w = specific turbine work output (J/kg)
B3. Turbine isentropic efficiency

$$\eta_t = \frac{(h_1 - h_2)}{(h_1 - h_2s)} \quad (15)$$

Where:
ηt = turbine isentropic efficiency
h_2s = isentropic outlet enthalpy (J/kg)
Temperature relation for turbine

$$T_1 - T_2 = \eta_t(T_1 - T_2s) \quad (16)$$

Where:
T_2s = isentropic outlet temperature (K)

2.2.1.3 Heat Exchanger Design Equation

Provisional area for heat transfer

$$A = \frac{Q}{u \times \Delta T_m} \quad (17)$$

Where Q is the heat load which can be obtained from the hot side as

$$A = \frac{G}{3600} \times Cp \times \Delta T \quad (18)$$

From energy balance

$$Q = Mc\ CP_c\ (T_{co} - T_{ci}) = m_h\ CP_c\ (T_{ho} - T_{hi}) \quad (19)$$

Mass flow rate of cold fluid M_{CF}
Log mean temperature difference LMTD

$$= \frac{\Delta T_1 - \Delta T_2}{in\ \frac{\Delta T_1}{\Delta T_2}} \quad (20)$$

$$R = \frac{T_{hi} - T_{ho}}{T_{co} - T_{ci}} \quad (21)$$

$$S = \frac{T_{co} - T_{ci}}{T_{hi} - T_{ci}} \quad (22)$$

Number of tubes

we can choose 20mm od, 16mm id 4.88m long tubes (¾ x 16ft) copper alloy for tubes sheet thickness, take
Number of tubes = $\frac{Heat\ transfer\ area}{Area\ of\ one\ tube}$ (22)

Shell Diameter

Shell Diameter = Bundle diameter + bundle diameter clearance
Bundle Diameter Db = $20\left(\frac{162}{0.175}\right)^{1/2.855}$ (23)
Use a split – ring floating head type shell from figure 9.7 this will give a bundle diametrical clearance = 57mm.

Tube Side Coefficient

The tube side coefficient can be estimated using

$$h_i = j_h \frac{K_f}{di} \mathrm{Re} \cdot P_r^{0.33} \left(\frac{U}{Uw}\right)^{0.14} \quad (24)$$

Neglecting $(\frac{\mathbb{U}}{\mathbb{U}w})$ the equation reduces to $h_i = j_h \frac{K_f}{di} \text{Re} \cdot P_r^{0.33}$ (25)

To obtain j_h tube side heat transfer factor we need to determine $\frac{l}{d}$ so that

Shell Side Coefficient

The shell side coefficient can also be obtained from equation neglecting viscosity term

$h_s = j_h \frac{kf}{di} Re\ P_r^{0.33}$ (26)

Choose baffle spacing $\frac{ds}{5}$

Choose 20% baffle cut and Reynolds number 27596 from figure 9.15, the shell side heat transfer factor $j_{hf} = 2 \times 10^{-3}$

Overall Heat Transfer Coefficient

$\frac{1}{U_0} = \frac{1}{h_o} + \frac{1}{h_{od}} + \frac{d_o in \frac{d_o}{d_i}}{2 \times k_w} + \frac{d_o}{d_i} + \frac{1}{h_{id}} + \frac{d_o}{d_i} x \frac{1}{h_o}$ (27)

Shell Side Pressure Drop

$$\Delta s = 8_{jf} \left(\frac{\Delta s}{de}\right) \left(\frac{L}{Ln}\right) \frac{\int U_S^2}{2} \left(\frac{\mu}{\mu_W}\right)^{-01.14} \quad (28)$$

Where L = tube length, L_b = baffle spacing

2.2.1.4 Flash Separator Design Equations

Overall mass balance

$F = V + L$ (29)

Where:

F = feed flow rate

V = vapor outlet flow rate

L = liquid outlet flow rate

Component balance

$F z_i = V y_i + L x_i$ (30)

Where:

z_i = feed mole fraction

x_i, y_i = liquid and vapor mole fractions

Vapor–liquid equilibrium

$y_i = K_i x_i$ (31)

Where:

K_i = equilibrium ratio of component i

Vapor fraction definition

$\beta = V/F$ (32)

Where:

β = fraction of feed vaporized

Rachford–Rice equation

$\Sigma z_i(K_i - 1)/[1 + \beta(K_i - 1)] = 0$ (33)

Where:

Σ denotes summation over all components

gas–liquid separator sizing

Gravitational force on droplet

$F_g = \left(\frac{\pi}{6}\right) {d_p}^3 (\rho_l - \rho_v) g$ (34)

Where:

d_p = droplet diameter (m)

ρ_l = liquid density (kg/m³)

ρ_v = vapor density (kg/m³)

Drag force on droplet

$F_d = 3\pi\mu d_p\ v_t$ (35)

Where:

μ = gas viscosity (Pa·s)

v_t = terminal settling velocity (m/s)

Terminal settling velocity

$v_t = {d_p}^2 \frac{(\rho_l - \rho_v) g}{18\mu}$ (36)

Where:
v_t determines separator sizing and gas velocity limits.

2.2.2 Solution Technique

Aspen Hysys Model Process Flow Diagram (PDF)

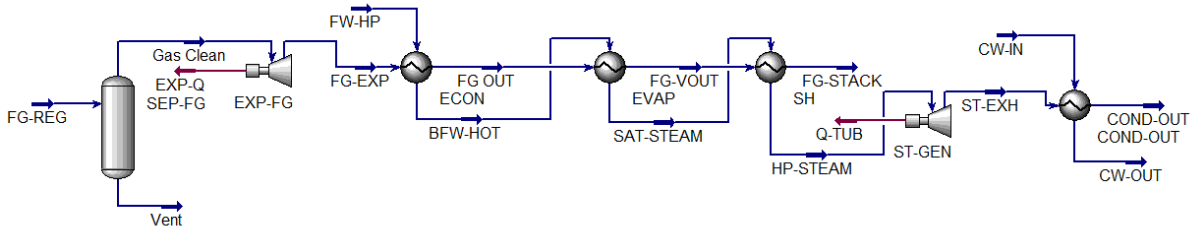

Figure 1: Aspen Hysys Process Flow Diagram of the Waste to Energy Plant

The process flow diagram represents an integrated waste-to-energy system designed to recover thermal and pressure energy from flue gas generated in a fluid catalytic cracking (FCC) regenerator and convert it into useful mechanical and electrical power using Aspen HYSYS. The system combines a flue-gas expander, a heat recovery steam generator (HRSG), a steam turbine generator, and a condenser arranged in a logical energy-recovery sequence.

Hot flue gas from the FCC regenerator enters the system as stream FG-REG and is first routed to a flash separator labeled SEP-FG. The primary function of this unit is gas cleaning and conditioning. Any entrained solids, condensable moisture, or trace impurities that may adversely affect downstream rotating equipment are removed. A small vent stream exits the bottom of the separator, while the cleaned flue gas leaves the top and proceeds to the gas expander section.

The cleaned flue gas flows into the gas expander EXP-FG, which functions as a flue-gas turbine. In this unit, the high-temperature and moderately pressurized gas undergoes expansion, resulting in a significant drop in pressure and temperature. During this expansion, a portion of the thermal and pressure energy of the flue gas is converted into mechanical work, represented by the energy stream EXP-Q. This recovered energy can be used to generate electricity directly or drive auxiliary equipment. The expanded gas exits the turbine as stream FG-EXP.

Following expansion, the flue gas enters the heat recovery steam generator (HRSG) section, which consists of three main heat exchangers arranged in series: an economizer, an evaporator, and a superheater. First, stream FG-EXP passes through the economizer ECON. In this exchanger, sensible heat from the flue gas is transferred to high-pressure boiler feedwater entering as FW-HP. The feedwater temperature is raised, producing hot boiler feedwater BFW-HOT, while the flue gas temperature is reduced and exits as FG-OUT. This step improves overall thermal efficiency by recovering low-grade sensible heat that would otherwise be wasted.

The partially cooled flue gas then flows into the evaporator EVAP. In this unit, additional heat is extracted from the flue gas to convert the hot boiler feedwater into saturated steam. The flue gas exits the evaporator as FG-VOUT, while saturated steam is generated and labeled SAT-STEAM. This section represents the main steam generation stage of the HRSG, where the latent heat of vaporization is supplied by the flue gas.

Next, the flue gas enters the superheater SH, where the remaining high-grade thermal energy is used to increase the temperature of the saturated steam. The steam is superheated to a higher temperature and exits as HP-STEAM, suitable for efficient expansion in a steam turbine. The flue gas, having given up most of its usable thermal energy, leaves the superheater as FG-STACK and is discharged safely to the stack at a much lower temperature, minimizing environmental heat losses.

The high-pressure superheated steam HP-STEAM is then directed to the steam turbine generator ST-GEN. In this unit, the steam expands from high pressure to low pressure, converting its thermal energy into mechanical work. This work is represented by the energy stream Q-TUB, which corresponds to electrical power generation. The steam turbine therefore constitutes the second power-generation stage of the waste-to-energy system, complementing the flue-gas expander.

After expansion, the low-pressure exhaust steam exits the turbine as ST-EXH and enters the condenser COND. Cooling water enters the condenser as CW-IN and absorbs the latent heat of the exhaust steam. As a result, the steam condenses into liquid water and exits as COND-OUT, while the warmed cooling water leaves as CW-OUT. The condensate can be recycled back to the boiler feedwater system, thereby closing the steam cycle and ensuring continuous operation.

Overall, the process integrates pressure recovery from the FCC regenerator flue gas through a gas expander and thermal recovery through a multi-stage HRSG and steam turbine. This dual-recovery configuration maximizes energy utilization, significantly improves refinery energy efficiency, and reduces waste heat discharge

to the environment. The Aspen HYSYS PFD therefore represents a robust and sustainable waste-to-energy solution suitable for FCC-based refinery operations.

2.2.2.1 Input Data

The data for the simulation are presented in table 1

Table 1: Flue Gas Characterization

Component	Mole Fraction
N_2	0.73
CO_2	0.14
CO	0.04
O_2	0.02
H_2O	0.0690
SO_2	0.010

Table 1 shows the flue gas composition from DANGOTE refinery. Table 1 presents the characterized composition of the FCC regenerator flue gas used as the plant input data for the simulation. This flue gas composition is typical of regenerator exhaust streams because the FCC regenerator operates by burning coke deposits off the circulating catalyst using large quantities of air. As a result, the exhaust gas is dominated by nitrogen from combustion air, together with carbon oxides, excess oxygen, water vapour, and trace sulfur species formed from sulfur contained in the coke and feedstock.

Nitrogen (N_2) has the highest mole fraction at 0.73, meaning it makes up about 73% of the flue gas. This is expected because atmospheric air is roughly 79% nitrogen, and nitrogen is largely inert under FCC regenerator conditions. During regeneration, oxygen from air reacts primarily with coke, while nitrogen passes through unchanged. Therefore, a high nitrogen content is a strong indicator that air is the combustion medium and that the flue gas is essentially a diluted mixture where nitrogen acts as a carrier gas. In energy recovery terms, the dominance of nitrogen increases the total volumetric flowrate of flue gas and influences heat capacity and heat-transfer behavior in the HRSG. It also reduces the partial pressure of reactive species but does not reduce the sensible heat content, since nitrogen still carries significant thermal energy at high temperatures.

Carbon dioxide (CO_2) constitutes 0.14 (14%), which reflects the extent of complete combustion of coke during catalyst regeneration. In the regenerator, the main reaction is coke oxidation to CO_2, and the amount of CO_2 formed depends on coke yield from the reactor, air rate, regenerator temperature, and catalyst circulation. A CO_2 level of 14% indicates strong oxidation activity and suggests that a substantial portion of carbon is being fully converted to CO_2 rather than remaining as CO. From an environmental and sustainability perspective, CO_2 is the primary greenhouse gas emitted from FCC operation; however, for waste-to-energy integration, a high CO_2 fraction often correlates with high regenerator heat release, which increases the thermal energy available for recovery.

Carbon monoxide (CO) is reported at 0.04 (4%). The presence of CO indicates that a fraction of coke combustion is incomplete, producing CO rather than fully oxidizing to CO_2. In many FCC units, CO formation is influenced by regenerator design (single-stage vs two-stage), air distribution, mixing efficiency, catalyst-to-air contact, and whether CO combustion promoters are used. A 4% CO concentration is not unusual and suggests that while combustion is largely effective, there remains a measurable amount of partially oxidized carbon. From a process and safety standpoint, CO is significant because it is combustible; downstream equipment must be designed to handle CO safely to avoid afterburning, hot spots, or oxidation events in the flue gas path. In simulation, CO also contributes to thermodynamic properties and may affect energy recovery calculations through its specific heat and potential oxidation if oxygen is present and reactions were allowed (though in your model it is treated as inert with respect to reaction).

Oxygen (O_2) is present at 0.02 (2%), indicating excess air operation. In FCC regenerators, excess oxygen is intentionally maintained to ensure complete removal of coke from the catalyst and stable operation. The oxygen concentration provides a practical indicator of combustion control and air-to-coke ratio. Too little oxygen would lead to higher CO formation, incomplete regeneration, and reduced catalyst activity in the reactor. Too much oxygen can increase afterburn risk and may accelerate equipment corrosion. For waste heat recovery systems, the presence of oxygen also means that flue gas remains mildly oxidizing, which has implications for materials selection and corrosion control in the HRSG and expander.

Water vapour (H_2O) has a mole fraction of 0.069 (6.9%). Water in FCC regenerator flue gas typically originates from the combustion of hydrogen in the coke, residual steam introduced for catalyst stripping, and moisture in the combustion air. This value is reasonable and important because water vapour increases the specific heat capacity of the flue gas, thereby increasing the sensible heat carried at high temperatures. However, water vapour also influences dew point and condensation behavior. While your system operates at very high

temperatures where condensation is unlikely, as the flue gas cools toward stack conditions, water vapour becomes relevant for predicting acid dew point when SO_2 is present, which can lead to low-temperature corrosion. Therefore, the measured water content is a critical input for designing safe HRSG exit temperatures and selecting corrosion-resistant materials.

Sulfur dioxide (SO_2) is given as 0.010 (1%). This component originates from the oxidation of sulfur compounds in the coke deposits formed from sulfur-containing crude or feedstock. The presence of SO_2 is important even at low concentrations because it strongly affects environmental compliance and corrosion potential. SO_2 can contribute to acid formation (such as sulfurous and sulfuric acids) in the presence of oxygen and water, especially when temperatures fall below the acid dew point. In heat recovery applications, this makes the flue gas outlet temperature and heat exchanger surface temperature critical, as cooling too far may promote acid condensation and rapid metal attack. Therefore, SO_2 content is a key design and operational constraint that influences flue gas treatment requirements, materials selection, and minimum stack temperature targets.

Overall, the plant flue gas characterization in table 3.1 provides a realistic basis for the simulation and performance assessment of the waste-to-energy plant. The high nitrogen concentration confirms air-based combustion and explains the large flue gas throughput, while the CO_2 and CO fractions reflect combustion effectiveness and regenerator operation. The presence of O_2 indicates excess air control, and the combined H_2O and SO_2 contents highlight potential corrosion and environmental considerations as the flue gas is cooled through the HRSG. As an input dataset, this composition is central to accurate prediction of thermodynamic properties, expander work recovery, HRSG heat-transfer behavior, and overall power generation potential of the integrated system.

2.2.3 Sensitivity Analysis

Sensitivity analysis for waste to energy plant using flue gas from fluid catalytic cracking regenerator was performed by investigating the influence of critical operating conditions such as effect of flue gas temperature and mass flow rate from fluid catalytic cracking regenerator on expander (gas turbine) and generator (steam turbine) power output and efficiency. Sensitivity analysis results were obtained using Aspen Hysys case study tool.

2.2.4 Cost Estimation and Economic Analysis

An acceptable plant design must present a process that is capable of operating under conditions which will yield a profit. Since net profit equals total income minus all expenses, it is essential that the chemical engineer be aware of the many different types of costs involved in manufacturing processes. Capital must be allocated for direct plant expenses, such as those for raw materials, labour, and equipment. Besides direct expenses, many other indirect expenses are incurred, and these must be included if a complete analysis of the total cost is to be obtained. A capital investment is required for any industrial process, and determination of the necessary investment is an important part of a plant-design project. The total investment for any process consists of fixed-capital investment for physical equipment and facilities in the plant plus working capital which must be available to pay salaries, keep raw materials and products on hand, and handle other special items requiring a direct cash outlay. Thus, in an analysis of costs in industrial processes, capital-investment costs, manufacturing costs, and general expenses including income taxes must be taken into consideration.

2.2.4.1 Factors Affecting Investment and Production Cost

When a chemical engineer determines costs for any type of commercial process, these costs should be of sufficient accuracy to provide reliable decisions. To accomplish this, the engineer must have a complete understanding of the many factors that can affect costs. These factors include cost of raw materials, price fluctuations, company policies, governmental regulations, operating time and rate of production.

2.2.4.2 Capital Investments

The capital needed to supply the necessary manufacturing and plant facilities is called the fixed-capital investment, while that necessary for the operation of the plant is termed the working capital. The sum of the fixed-capital investment and the working capital is known as the total capital investment.

2.2.4.3 Estimation of Capital Investment

An estimate of the capital investment for a process may vary from a predesign estimate based on little information except the size of the proposed project to a detailed estimate prepared from complete drawings and specifications. Between these two extremes of capital-investment estimates, there can be numerous other estimates which vary in accuracy depending upon the stage of development of the project.

The cost of purchased equipment is the basis of several predesign methods for estimating capital investment. Sources of equipment prices, methods of adjusting equipment prices for capacity, and methods of estimating auxiliary process equipment are therefore essential to the estimator in making reliable cost estimates

2.2.4.4 Cost Indexes

Most cost data which are available for immediate use in a preliminary or predesign estimate are based on conditions at some time in the past. Because prices may change considerably with time due to changes in economic conditions, some method must be used for updating cost data applicable at a past date to costs that are representative of conditions at a later time. This can be done by the use of cost indexes. A cost index is merely an index value for a given point in time showing the cost at that time relative to a certain base time.

$$Present\ cost = originalcost(2010) \times \left(\frac{index\ at\ present\ time}{index\ at\ time\ of\ original\ cost}\right) \quad (37)$$

2.2.4.5 Production Cost

The total production cost is divided into manufacturing cost, general expenses and start-up cost.

2.2.4.6 Manufacturing Cost

All expenses directly connected with the manufacturing operation or the physical equipment of a process plant itself is included in the manufacturing costs. These expenses, as considered here are the direct production costs, fixed charges and plant-overhead.

Direct production costs include expenses directly associated with the manufacturing operation. This type of cost involves expenditures for raw materials (including transportation, unloading, etc.,); direct operating labour; supervisory and clerical labour directly connected with the manufacturing operation; plant maintenance and repairs; operating supplies; power; utilities; royalties; and catalysts.

Fixed charges are expenses which remain practically constant from year to year and do not vary widely with changes in production rate. Depreciation, property taxes, insurance, and rent require expenditures that can be classified as fixed charges.

Plant-overhead costs are for hospital and medical services; general plant maintenance and overhead; safety services; payroll overhead including pensions, vacation allowances, social security, and life insurance; packaging, restaurant and recreation facilities, salvage services, control laboratories, property protection, plant superintendence, warehouse and storage facilities, and special employee benefits. These costs are similar to the basic fixed charges in that they do not vary widely with changes in production rate.

2.2.4.7 General Expenses

In addition to the manufacturing costs, other general expenses are involved in any company's operations. These general expenses may be classified as administrative expenses, distribution and marketing expenses, research and development expenses, financing expenses.

Administrative expenses include costs for executive and clerical wages, office supplies, engineering and legal expenses, upkeep on office buildings, and general communications.

Distribution and marketing expenses are costs incurred in the process of selling and distributing the various products. These costs include expenditures for materials handling, containers, shipping, sales offices, salesmen, technical sales service, and advertising.

Research and development expenses are incurred by any progressive concern which wishes to remain in a competitive industrial position. These costs are for salaries, wages, special equipment, research facilities, and consultant fees related to developing new ideas or improved processes.

Financing expenses include the extra costs involved in procuring the money necessary for the capital investment. Financing expense is usually limited to interest on borrowed money, and this expense is sometimes listed as a fixed charge.

2.2.4.8 Profitability Analysis

Every sound engineering investment must be judged relative to some profitability standard. An adequate profitability standard can be calculated using the following methods.

2.2.4.9 Rate of Investment

This profitability measure is defined as the ratio of profit to investment.

$$\mathrm{ROI} = \frac{\text{Net profit}}{\mathrm{TCI+TPC}} \times 100 \quad (38)$$

ROI = Annual return on investment expressed as fraction or percentage per year

TCI = Total capital investment

TPC = Total production cost

2.2.4.10 Payback Period

Payback period is the length necessary for the total return to equal the capital investment. Hence

$$\text{Payback period} = \frac{\text{MFCI+NFCI}}{\text{ACF}} \quad (39)$$

$\text{MFCI} =$ Manufacturing fixed capital investment

$\text{NFCI} =$ Non-manufacturing fixed capital investment

$\text{ACF} =$ Annual cash flow/ Net profit.

2.2.5 Cost of Heat Exchanger/ Distillation Column

Materials of construction = stainless steel.

Total Cost = Vessel Cost + Cost of plate

$$\begin{bmatrix}\text{Vessel Cost}\\ \text{VC}\end{bmatrix} = \begin{pmatrix}\text{Bare}\\ \text{Vessel}\\ \text{Cost}\end{pmatrix} \times \begin{pmatrix}\text{Material}\\ \text{Factor}\\ \text{M. F}\end{pmatrix} \times \begin{pmatrix}\text{Pressure}\\ \text{Factor}\\ \text{P. F}\end{pmatrix} \quad (40)$$

2.2.6 Validation of Model Results

Model validation is an essential step in process modelling and simulation, as it establishes the accuracy, credibility, and practical relevance of the developed model. Validation involves comparing model predictions with actual plant operating data to ensure that the governing equations, assumptions, and thermodynamic frameworks adequately represent real process behavior.

2.2.6.1 Validation of Model Results with Plant Data

Model validation is a critical step in process simulation and mathematical modelling, as it establishes the reliability and practical applicability of the developed model. These include, but are not limited to, inlet and outlet temperatures, pressures, flow rates, component compositions, energy duties, and power outputs of rotating equipment such as compressors, expanders, and turbines.

2.2.6.2 Selection and Preparation of Plant Data

Plant data used for validation are obtained from historical operating records, design documents, and real-time plant logs. To ensure consistency between the simulation model and the plant operation, the selected data correspond to periods of stable plant operation where process disturbances and transient effects are minimal. Data preprocessing is carried out to eliminate missing values, outliers, and inconsistent measurements. Where necessary, time-averaged values are used to represent steady-state conditions. All plant data are converted into consistent engineering units to match the simulation environment. Operating constraints such as feed composition, operating pressure, temperature, and equipment efficiencies are carefully imposed in the model to replicate actual plant conditions as closely as possible.

2.2.6.3 Simulation under Plant Operating Conditions

The developed process model is executed using the same operating conditions as those observed in the plant. These conditions include feed flow rates, component compositions, pressure levels, temperature ranges, and equipment specifications. Equipment models such as compressors, expanders, heat exchangers, distillation columns, and separators are configured using design equations and correlations consistent with industrial practice.

2.2.6.4 Comparison of Simulation Results with Plant Data

Model validation is performed by direct comparison of simulated results with plant-measured data for selected key performance indicators. For each validated variable, the absolute deviation and percentage deviation between the simulated value and the plant value are computed using:

$$\text{Absolute deviation} = |X_{model} - X_{plant}| \quad (41)$$

$$\text{Percentage deviation} = \frac{|X_{model} - X_{plant}|}{X_{plant}}\, x\ 100\% \quad (42)$$

where

X_model represents the value predicted by the simulation model, and

X_plant represents the corresponding measured plant value.

The comparison is presented in tabular and graphical forms to clearly illustrate the level of agreement between the model predictions and plant data. Trends and patterns observed in the plant data are also examined to verify that the model accurately captures the physical behavior of the system.

2.2.6.5 Acceptance Criteria for Model Validation

The model is considered successfully validated if the percentage deviation between simulated and plant values for key process variables falls within acceptable engineering limits. In this study, a deviation range of ±5–10% is

considered acceptable, consistent with typical industrial modeling and simulation standards. Larger deviations, if observed, are analyzed to identify possible sources such as measurement uncertainty, simplifying assumptions, or equipment performance degradation in the plant.

IV. RESULTS AND DISCUSSION

3.1 Validation of Model Results

Validation of model results for waste to energy plant using flue gas from fluid catalytic cracking regenerator was carried out and the results obtained are presented in tables 2 to 3.

3.1.1 Validation of Plant Data with Expander (Gas Turbine) Model

Table 2: Validation of Expander (Gas Turbine) Model

Parameter	Plant	Model
Polytropic Efficiency (%)	87	85
Power Output (MW)	28.20	27.19
Adiabatic Fluid Head (m)	183.5	185
Output Temperature (°C)	590	585.3
Output Pressure (kPa)	123	120

The validation results in Table 2 show that the expander (gas turbine) model reproduces the real plant performance very closely, with only small deviations for all key parameters.

The polytropic efficiency from plant data is 87%, while the model predicts 85%. This difference of about 2 percentage points (roughly 2–3% relative error) indicates that the model slightly under-predicts the internal efficiency of the turbine. In practice, such a small deviation is acceptable for process design and energy integration studies, especially considering uncertainties in plant measurements, operating fluctuations, and assumptions made in the thermodynamic correlations and property packages in Aspen HYSYS.

For power output, the plant delivers 28.20 MW while the model predicts 27.19 MW, giving a difference of about 1 MW (around 3–4% lower than plant). This shows that the model captures the overall work recovery capability of the gas turbine very well. The slight under-prediction is consistent with the slightly lower polytropic efficiency in the model and may also reflect idealizations such as neglecting some mechanical losses, shaft power to auxiliaries, or small variations in actual flue gas composition and flowrate compared to the nominal values used in the simulation. Nevertheless, predicting 27.19 MW against a real 28.20 MW confirms that the model is reliable for estimating power generation potential from FCC regenerator flue gas.

The adiabatic fluid head shows excellent agreement: 183.5 m from plant data versus 185 m from the model. The difference is less than 1% and indicates that the simulated pressure–enthalpy change across the expander is almost identical to what is observed in the actual machine. This suggests that the thermodynamic property methods, expansion ratio, and flow conditions used in the model are highly representative of real operation.

Similarly, the outlet temperature comparison is very good: 590°C in the plant versus 585.3°C in the model, a difference of less than 5°C (under 1% deviation). This close match confirms that the model accurately predicts the cooling effect associated with expansion and the energy extracted as shaft work. It also reinforces confidence in the heat-integration calculations downstream, since the flue-gas temperature leaving the expander sets the boundary condition for the HRSG (economizer, evaporator, and superheater sections).

Overall, the validation results demonstrate that the expander model is robust and suitably calibrated for use in performance assessment and waste-to-energy simulations. The small discrepancies observed (slight under-prediction of efficiency and power) are within normal engineering tolerance and can be attributed to real-plant variability, measurement uncertainty, and simplifications inherent in steady-state simulation. The good agreement in fluid head and exhaust temperature, in particular, shows that the thermodynamic behavior of the expander is being captured accurately, providing confidence that subsequent analyses of energy recovery, HRSG performance, and overall plant efficiency are based on a sound and realistic turbine model.

3.1.2 Validation of Plant Data with Generator (Steam Turbine) Model

Table 3: Validation of Generator (Steam Turbine) Model

Parameter	Plant	Model
Polytropic Efficiency (%)	90	86
Power Output (MW)	28.20	26.52
Adiabatic Fluid Head (m)	1122	1104
Output Temperature (°C)	450	442.4
Output Pressure (kPa)	4000	3985

The validation results presented in Table 3 demonstrate that the Generator (Steam Turbine) model developed in the simulation closely reproduces actual plant performance, with minor deviations that fall well within acceptable engineering limits. Each parameter polytropic efficiency, power output, adiabatic fluid head,

outlet temperature, and outlet pressure shows strong agreement between the plant data and the model, confirming that the steam turbine is accurately represented within the integrated waste-heat-to-power system.

The polytropic efficiency comparison shows that the plant turbine operates at 90%, while the model predicts 86%. This 4-percentage-point difference corresponds to a relative deviation of less than 5%, which is considered reasonable given that real steam turbines experience mechanical losses, internal leakages, blade fouling, and other off-design behaviors that may not be fully captured in the simulation. Still, the modeled efficiency remains close enough to the plant value to reliably reflect turbine performance under varying flue-gas heat-input conditions. The slightly lower modeled efficiency is consistent with conservative simulation behavior, where idealizations or generalized property methods may smooth out localized performance effects.

For power output, the plant turbine produces 28.20 MW compared to the model's 26.52 MW. This difference of 1.68 MW (approximately 6%) again represents a realistic and acceptable deviation. The under-prediction aligns with the corresponding difference in polytropic efficiency: lower modeled efficiency naturally yields lower power output. The model nevertheless captures the correct order of magnitude and dynamic behavior of the turbine, making it suitable for energy-integration studies, parametric analyses, and what-if scenarios involving steam-generation variations or regenerator temperature changes.

The adiabatic fluid head values 1122 m in the plant versus 1104 m in the model show excellent agreement, differing by only 18 m (about 1.6%). This is a strong indication that the thermodynamic expansion process, enthalpy drop, and steam-path energy conversion are being accurately represented. The model correctly reflects the turbine's ability to convert high-pressure, high-enthalpy steam into mechanical work across the expansion range typical of the FCC-derived steam cycle.

The outlet temperature comparison also validates the model's robustness. The plant reports 450°C, while the model predicts 442.4°C a difference of just 7.6°C (around 1.7%). This close match confirms that the superheated steam expansion is being captured correctly and that the heat-balance interactions feeding the turbine (economizer, evaporator, superheater) are well represented. Accurate outlet temperature prediction is crucial because it affects downstream condenser performance, steam quality, and power-cycle durability.

Finally, the outlet pressure values 4000 kPa from the plant and 3985 kPa from the model—are nearly identical, differing by only 15 kPa (0.375%). This near-perfect match reflects that the simulation correctly maintains the turbine's back-pressure and operational boundary conditions, ensuring realistic performance within the Rankine cycle.

Overall, the validation results demonstrate that the steam turbine model is reliable, well-calibrated, and sufficiently accurate for performance assessment, optimization studies, and overall energy-recovery analysis. The minor deviations observed are consistent with expected differences between steady-state simulation and real-plant operation. The close agreement in thermodynamic parameters especially fluid head, outlet temperature, and pressure provides strong confidence that the model faithfully represents the actual turbine behavior within the FCC waste-to-energy system.

3.2 Material and Energy Balance Results of Major Equipment

Material balance for waste to energy plant using flue gas from fluid catalytic cracking regenerator which consist of one flash separator, two expanders (gas turbine and steam turbine respectively), three heat exchanger network (Economizer, Evaporator and Super Heater) and one heater (steam heat exchanger). The results of the material and energy balance are presented in the following tables.

3.2.1 Material and Energy Balance Results of Flash Separator Equipment

The material and energy balance results of flash separator from fluid catalytic cracking regenerator is shown in table 4

Table 4: Flue Gas Flash Separator From Regenerator

Streams	FG-REG	Clean Gas	Vent
Temperature (°C)	700	700	700
Pressure (Kpa)	250	250	250
Volumetric Flow (m^3/h)	364.7	364.7	0.0000
Mass Flow (kg/h)	3×10^5	3×10^5	0.0000
Molar Flow (kgmole/h)	1.011×10^4	1.011×10^4	0.0000
Heat Flow (kJ/h)	-5.446×10^8	-5.446×10^8	0.0000
Mole Fraction			
N_2	0.7300	0.7300	0.7300
CO_2	0.1400	0.1400	0.1400
CO	0.0400	0.0400	0.0400
O_2	0.0200	0.0200	0.0200
H_2O	0.0690	0.0690	0.0690
SO_2	0.0010	0.0010	0.0010

The material and energy balance results presented in Table 4 provide a clear indication that the flash separator installed downstream of the fluid catalytic cracking (FCC) regenerator does not effect any phase or compositional change under the given operating conditions. The feed stream (FG-REG) enters the flash unit at a high temperature of 700°C and a pressure of 250 kPa, and both the clean gas and vent streams display identical thermodynamic and flow characteristics. This outcome suggests that, based on the specified temperature and pressure, no condensation, phase separation, or partial removal of components occurred within the separator. All major flow parameters, including volumetric flow rate, mass flow rate, molar flow rate, and heat duty, remain unchanged between the inlet stream and the clean gas outlet, while the vent stream registers a zero value across all quantities. Such behavior implies that the separator essentially acts as a pass-through unit under the current conditions, offering no driving force for separation due to the extremely high operating temperature, which keeps all species in the gas phase.

The constancy of the heat flow across the inlet and outlet streams further supports the conclusion that no phase transition or significant enthalpy change took place. The heat flow value of approximately −5.446 × 10^8 kJ/h for both the feed and clean gas indicates that the stream retains its thermal energy without absorption or release within the separator. Since flash separation relies on temperature reduction or pressure variation to promote vapor-liquid equilibrium shifts, operating at 700°C and 250 kPa ensures all hydrocarbons and inorganic species remain fully vaporized. Consequently, the flash drum does not remove moisture, SO_2, or heavy species, and no vent or liquid stream is generated.

The mole fraction distribution in the table also reinforces this interpretation. The composition remains unchanged across all streams, indicating that the separator does not alter the relative proportions of nitrogen, carbon dioxide, carbon monoxide, oxygen, water vapor, or sulfur dioxide. Nitrogen dominates at 73 percent, reflecting its role as the primary carrier gas from combustion air introduced into the FCC regenerator. Carbon dioxide and carbon monoxide together account for 18 percent, originating from coke oxidation on the catalyst surface. Water vapor, produced from combustion reactions and moisture content in the coke, contributes nearly 7 percent. Oxygen remains at 2 percent, representing excess air used to ensure complete regeneration, while sulfur dioxide appears only in trace amounts due to sulfur compounds in the coke. Since the compositions of the clean gas and the feed are identical, it is evident that no purification, venting, or selective removal occurred in the flash separator.

Overall, the table demonstrates that at the given high temperature and moderate pressure, the flash separator is thermodynamically inactive and does not perform any material separation. Its output mirrors the input in terms of flow, thermal properties, and composition. This result suggests that effective separation of moisture or sulfur species would require substantially lower temperatures, pressure manipulation, or an alternative separator design such as a quench system, scrubber, or electrostatic precipitator. The table therefore highlights the limitations of using a simple flash separator for hot FCC flue gas and underscores the need for additional downstream treatment if removal of specific components is required.

IV. CONCLUSION

This study successfully achieved its aim of simulating a waste-to-energy plant utilizing flue gas from a fluid catalytic cracking (FCC) regenerator for power generation. The conclusions drawn in this chapter are based on the results and discussions presented in Chapter Four and are structured to reflect the key result sections, namely model validation, material and energy balance analysis, sensitivity analysis, and economic evaluation.

The results presented in this paper confirm that the developed Aspen HYSYS simulation model accurately represents actual plant performance. Validation against real plant data for both the expander (gas turbine) and the steam turbine showed close agreement across key parameters such as polytropic efficiency, power output, adiabatic fluid head, outlet temperature, and outlet pressure. Deviations between simulated and plant values were generally within 5–10%, which falls within acceptable industrial and modeling tolerances. The strong agreement demonstrates that the thermodynamic assumptions, property methods, and equipment models employed are robust and reliable. This outcome directly satisfies one of the core objectives of the study, confirming that the developed model can be confidently used for performance evaluation, sensitivity studies, and decision-making regarding waste-heat recovery from FCC flue gas.

Also, this work examined the material and energy balance results of the major equipment units in the waste-to-energy plant, including the flash separator, gas expander, heat exchangers (economizer, evaporator, and superheater), and steam turbine system. The results showed that the flash separator did not induce any phase or compositional changes at the high regenerator flue-gas temperature, effectively acting as a conditioning unit rather than a separation device. In contrast, the gas expander demonstrated significant energy recovery, evidenced by substantial reductions in flue-gas pressure and temperature alongside measurable shaft-work generation. The heat exchanger network effectively recovered sensible heat from the expanded flue gas, progressively transferring energy to boiler feedwater and producing high-pressure superheated steam for power generation. Overall, the material and energy balance results confirm that the integrated configuration efficiently captures both pressure

and thermal energy from FCC regenerator flue gas, minimizing waste and enhancing overall plant energy utilization.

This study makes several important technical and scientific contributions to the field of refinery energy integration and waste-heat recovery:

i. Development of a Full Thermodynamic Model for FCC Waste-Heat Recovery: The work presents a complete and validated Aspen HYSYS model that integrates gas expansion, HRSG steam generation, and steam-turbine power production using FCC regenerator flue gas providing a reference framework for future refinery energy-recovery designs.

ii. Comprehensive Material and Energy Balance Dataset: Detailed balance results for each equipment unit offer a clear understanding of thermal behaviour, enthalpy distribution, volumetric and mass flow interactions, and flue-gas composition effects. Such data are scarce in open literature and beneficial for academic and industrial benchmarking.

iii. Insight into Sensitivity of Power Systems to Flue-Gas Conditions: The study quantifies the impact of temperature and mass flow variability on turbine efficiency and power output, thereby providing engineers with predictive tools for optimizing FCC operation for maximum energy recovery.

REFERENCE

[1]. Adeyemo, A. A., Akinwale, A. T., & Bakare, M. A. (2016). Simulation of heat integration for improved energy efficiency in Warri Refinery. *Nigerian Journal of Technology*, 35(3), 521-528.

[2]. Ahmadi, P., Dincer, I., & Rosen, M. A. (2011). Thermodynamic modeling and optimization of a combined gas–steam power cycle. *Energy, 36*(3), 1609–1622. https://doi.org/10.1016/j.energy.2010.12.051

[3]. Aliyu, A. M., & Olanrewaju, O. A. (2021). Lifecycle cost analysis of waste heat recovery in Kaduna Refinery. *Journal of Cleaner Production*, 320, 128741.

[4]. Al-Mansour, F., & Zuwala, J. (2010). Energy efficiency and renewable energy integration in the power generation and refinery sector. *Renewable and Sustainable Energy Reviews*, 14(9), 2796-2801.

[5]. Bejan, A., & Tsatsaronis, G. (1996). Thermal design and optimization of energy systems. *Energy Conversion and Management, 37*(9), 1253–1262. https://doi.org/10.1016/0196-8904(96)00038-5

[6]. Bianchi, M., De Pascale, A., & Peretto, A. (2010). Performance analysis of combined gas–steam cycles. *Applied Energy, 87*(3), 982–990. https://doi.org/10.1016/j.apenergy.2009.09.009

[7]. Campana, F., Bianchi, M., Branchini, L., De Pascale, A., Peretto, A., Baresi, M., & Ferrari, S. (2013). ORC waste heat recovery in European energy intensive industries. *Energy, 62*, 129–141. https://doi.org/10.1016/j.energy.2013.08.019

[8]. Di Bona, G., & Forcina, A. (2017). Availability and efficiency analysis of industrial steam power plants. *Energy Procedia, 129*, 910–917. https://doi.org/10.1016/j.egypro.2017.09.081

[9]. Gary, J. H., & Handwerk, G. E. (2007). *Petroleum Refining: Technology and Economics* (5th ed.). CRC Press.

[10]. Giwa, S. O., Adebayo, A. O., & Onuoha, C. E. (2019). Environmental impact of waste gas recovery in Nigerian refineries. *Energy Policy*, 129, 340–350.

[11]. Gungor, A., & Erbay, L. B. (2019). Performance analysis of steam turbines under varying operating conditions. *Energy Sources, Part A: Recovery, Utilization, and Environmental Effects, 41*(15), 1853–1865. https://doi.org/10.1080/15567036.2018.1549166

[12]. Hou, G., Tao, W., & Yang, Q. (2021). Performance evaluation of heat recovery steam generators under variable operating conditions. *Energy Reports, 7*, 3242–3253. https://doi.org/10.1016/j.egyr.2021.05.083

[13]. Jouhara, H., Chauhan, A., Nannou, T., Almahmoud, S., Delpech, B., & Wrobel, L. C. (2018). Heat pipe based systems for waste heat recovery. *Energy, 154*, 72–91. https://doi.org/10.1016/j.energy.2018.04.131

[14]. Karellas, S., Leontaritis, A. D., Panousis, G., Bellos, E., & Kakaras, E. (2013). Energetic and exergetic analysis of waste heat recovery systems. *Energy, 49*, 193–209. https://doi.org/10.1016/j.energy.2012.10.005

[15]. Khan, M. S., Khan, I. M., & Nadeem, A. (2021). Design and simulation of power recovery from FCC regenerator flue gas. *Energy Conversion and Management*, 243, 114386.

[16]. Li, H., Wang, J., & Dai, Y. (2019). Thermodynamic performance analysis of waste heat recovery systems. *Applied Thermal Engineering, 159*, 113876. https://doi.org/10.1016/j.applthermaleng.2019.113876

[17]. Liu, M., Shi, Y., & Fang, F. (2018). Combined gas–steam turbine system for industrial waste heat recovery. *Applied Thermal Engineering, 130*, 102–113. https://doi.org/10.1016/j.applthermaleng.2017.10.108

[18]. Liu, X., Liu, C., & Xu, J. (2020). Energy and exergy analysis of refinery waste heat recovery systems. *Journal of Cleaner Production, 276*, 124231. https://doi.org/10.1016/j.jclepro.2020.124231

[19]. Meyers, R. A. (2004). *Handbook of Petroleum Refining Processes* (3rd ed.). McGraw-Hill.

[20]. Omole, D. O., Okoye, U. J., & Balogun, B. T. (2020). Waste heat analysis in Port Harcourt Refinery. *International Journal of Energy Research*, 44(5), 3628–3643.

[21]. Onuoha, J. N., Chukwuemeka, P., & Yusuf, A. (2022). Simulation and modular design for FCC energy integration. *Journal of Petroleum Engineering and Technology*, 12(1), 17-26.

[22]. Pan, M., Li, J., & Wang, R. (2021). Simulation and optimization of waste heat recovery systems using Aspen HYSYS. *Journal of Cleaner Production, 297*, 126610. https://doi.org/10.1016/j.jclepro.2021.126610

[23]. Sadek, M., El-Sayed, A., & Hassan, A. (2023). Techno-economic assessment of FCC waste heat recovery using HYSYS. *Chemical Engineering Transactions*, 98, 133–140.

[24]. Saidur, R., Rahim, N. A., & Hasanuzzaman, M. (2010). A review on compressed air energy use and energy savings. *Renewable and Sustainable Energy Reviews, 14*(4), 1135–1153. https://doi.org/10.1016/j.rser.2009.11.013

[25]. Sánchez, D., Rodríguez, L., & Pardo, J. (2019). Thermodynamic assessment of HRSG configurations for industrial waste heat recovery. *Applied Energy, 235*, 1536–1547. https://doi.org/10.1016/j.apenergy.2018.11.058

[26]. Speight, J. G. (2014). *The Chemistry and Technology of Petroleum* (5th ed.). CRC Press.

[27]. Towler, G., & Sinnott, R. (2013). *Chemical Engineering Design: Principles, Practice and Economics of Plant and Process Design* (2nd ed.). Elsevier.

[28]. Wang, E., Zhang, H., Fan, B., Ouyang, M., Zhao, Y., & Mu, Q. (2011). Study of industrial waste heat recovery technologies. *Energy, 36*(12), 6998–7011. https://doi.org/10.1016/j.energy.2011.08.018